Rock Mechanics and Rock Engineering (2019) 52:4889–4905
https://doi.org/10.1007/s00603-019-01915-4

ORIGINAL PAPER

Stability Analysis of Rock Structure in Large Slopes and Open-Pit Mine: Numerical and Experimental Fault Modeling

Babak Azarfar[1] · Seyedsaeid Ahmadvand[1] · Javad Sattarvand[1] · Behrooz Abbasi[1]

Received: 31 October 2018 / Accepted: 15 June 2019 / Published online: 27 July 2019

Abstract

Deep open-pit mines and large rock slopes expose many diverse rock lithologies and geological structures (e.g., faults, bedding planes) that may reduce the integrity of slopes. Numerical modeling is a powerful tool for simulating these structures; however, there are few guidelines and methods for calibrating/validating and implementing faults in a numerical model. This paper presents a novel laboratory method to calibrate numerical models and highlights the challenges in simulating faults. One of the main issues in reliable modeling of faulted rock structure is the scarcity of experimental analyses in the laboratory under the controlled conditions. Moreover, a comprehensive evaluation of the effect of using the conventional fault modeling methods on the stability of rock structures is required, as well as a benchmarking between theoretical and experimental results. This research combines theory and experiment, to fill the existing gaps, using numerical simulation and laboratory measurements. Using FLAC3D software, the sensitivity and comparative analyses are carried out for the numerical simulations to investigate the stability of rock slopes on large and small scales (overall open-pit slope and bench slope), and the fault zones. The weak zone (WZ), ubiquitous-joint (UJ), and interface (IF) techniques are the widely used methods in the modeling to capture fault slip mechanisms. The factor of safety (FOS) of the slope is monitored upon variation of the design parameters, such as fault and rock mass mechanical properties, fault types, and modeling framework (e.g., mesh density, convergence ratio). In addition, parameters such as shear displacement and shear stress are investigated to deduce the failure mechanism of the studied models. Finally, laboratory tests were performed to calibrate the modeling results and approximate the agreement between theoretical and experimental results. The results of sensitivity analysis showed that choosing an adequately low convergence ratio is critical for estimating FOS. However, beyond a certain convergence ratio, below 10^{-7}, this change is negligible (less than 5%). The results of mesh density sensitivity analysis indicate that the FOS values are insensitive to the mesh density in the WZ method (less than 5% change in FOS), the IF method shows the median sensitivity (5–12% change in FOS), and the UJ method is the most sensitive (FOS values improves by ~ 31%). Comparison between laboratory test and numerical modeling ($FOS_{lab} = 1.71$, $FOS_{WZ} = 1.51$, $FOS_{IF} = 1.62$, and $FOS_{UJ} = 1.76$) indicates a good agreement between the UJ and IF methods and the laboratory model (~ 3–5% discrepancy). It needs to be mentioned that these analyses/tests are not to favor one method over the other, but rather to emphasize the pros and cons of each within the assumptions of this study.

Keywords Slope stability · Factor of safety · Sensitivity analysis · Fault modeling methods · Numerical modeling · Fault structure laboratory test

List of Symbols

$F_n^{(t+\Delta t)}$	Normal force at each implicit time step $(t + \Delta t)$ (N)
$F_{si}^{(t+\Delta t)}$	Shear force at each implicit time step $(t + \Delta t)$ (N)
Δu_{si}	Incremental relative shear displacement (m)
A	Area associated with the interface element (m^2)
k_n	Normal stiffness (Pa m^{-1})
k_s	Shear stiffness (Pa m^{-1})
ψ	Dilation angle (°)
φ	Friction angle (°)
c	Cohesion (Pa)
p	Pore pressure (Pa)
σ_{si}	Incremental shear stress vector due to interface stress initialization (Pa)

✉ Behrooz Abbasi
abbasi@unr.edu

[1] Department of Mining and Metallurgical Engineering, University of Nevada, Reno, Reno, NV 89557, USA

u_n Absolute normal penetration of the interface node into the target face (m)
β Angle of discontinuity (°)
φ_j Joint friction angle (°)
c_j Joint cohesion (Pa)
σ_n Normal stress (Pa)
τ Shear stress (Pa)
σ_1 Maximum principal stress (Pa)
σ_3 Minimum principal stress (Pa)
C_0 Initial cohesion (Pa)
φ_0 Initial internal friction angle (°)
C_r Updated cohesion (Pa)
φ_r Updated internal friction angle (°)
$|F_s|_o$ Magnitude of shear force (N)
σ_{ni} Incremental normal stress added due to interface stress initialization (Pa)
T_S Tensile strength (Pa)

1 Introduction

Slope stability analysis is a critical part of the mining and civil engineering designs, especially in open-pit mine and large slopes (e.g., dam). Slope failure may result in prolonged production interruption, fatality, and equipment loss (Duncan 1996; Stacey et al. 2003). With the growth of global demand for minerals, the depth of open-pit mines has increased significantly. This has imposed several design challenges in slope engineering and potentially increased the risk of large slope failures (Sjoberg et al. 2000; Stacey et al. 2003; Franz 2009; Tutluoglu et al. 2011).

In deep open-pit mines, complex rock lithologies are exposed, which interact with geological structures (e.g., faults, bedding planes) and impact the rock slope stability and impose significant design challenges for geotechnical engineers. The structural characteristics of the slope, such as geometry, geological features, and rock mass properties are some of the key factors affecting the slope stability (Stead and Wolter 2015). For instance, geological discontinuities such as faults, and their properties [shear strength properties, dip (D), and dip-direction (D-D)] determine the failure mechanism (Raghuvanshi 2019).

Several techniques are used in determining slope stability. Calculating the factor of safety (FOS), defined as the ratio of actual shear strength to the minimum shear stress required to maintain equilibrium (Eq. (1)), is a common approach to evaluate the slope stability in numerical modeling (Bishop 1955; Matsui and San 1992; Fleurisson 2012; Taleb Hosni and Berga 2016). In this definition, the FOS value of unity represents imminent failure.

$$\mathrm{FOS} = \frac{\text{Shear strength of rock mass or soil}}{\text{Shear stress required to prevent failure}}. \quad (1)$$

In numerical modeling, solve ratio is a unitless measurement to estimate the system stability. This ratio is defined as the sum of all out-of-balance force components at each node divided by the sum of all total forces applied at the similar node (Itasca 2017). As one of the commonly-used techniques, the shear strength reduction (SSR) method reduces the shear strength properties of the rock mass until a failure happens (Zienkiewicz et al. 1975; Duncan 1996; Dawson et al. 1999; Hammah et al. 2007; Yang et al. 2012; Gupta et al. 2016; You et al. 2017).

Dilation is another important factor in the failure analysis of soil rock and granular materials; dilation is defined as the volume change upon shear deformation (Vermeer 1998). Dilation becomes essential in the after-failure and plasticity analyses of the rock material. It has been demonstrated that dilation is interconnected with the cohesion and internal friction angle of the material (Alejano and Alonso 2005). Since the fault zone consists of weak material, such as gravel and soil, dilation is expected to affect the FOS of the slope. However, current methods consider dilation only after failure, and in this sense, they may overestimate the slope stability.

Numerical modeling is often used for simulating complex slope stability and fault effects, when analytical methods barely exist (Cala et al. 2006; Hammah et al. 2007; Tutluoglu et al. 2011; Zhang et al. 2011; Wiles 2014; Sun et al. 2016; Tang et al. 2017; Park and Michalowski 2017). However, there are few guidelines for fault simulation in numerical modeling due to difficulties in characterizing the fault slip mechanism (Mostyn et al. 1997; Zheng et al. 2013; Alzo'ubi 2016; Tang et al. 2017). Three widely-used numerical methods for fault modeling are weak zone (WZ), ubiquitous-joint (UJ), and interface (IF), each of which introduces the fault in a different manner (Azarfar 2019). In the WZ method, the fault material is treated as a weak zone (Fig. 1a) with no preferred weakness direction. The UJ method models the fault as a zone with a preferred weakness direction oriented in the direction of the fault plane (Fig. 1b). In this method, the dip angle and direction of the fault surface can be accurately implemented in the model (Fig. 2). In the IF method, the fault has zero thickness and fault elements contact at an interface (discontinuous face) which defines the fault direction (Fig. 1c).

The overall approach of slope stability analysis and fault materials simulation is shown in Fig. 3. The slope stability analysis has a different response with respect to the geometry, shear band, fault material properties and method used to model the faulted zone (WZ, UJ or IF). Model calibration/validation is an important step in any numerical modeling to obtain a representation within the acceptable margin of uncertainties. Currently, slope back analysis is the only method to calibrate the slope numerical models and evaluate fault shear strength (Azarfar 2019). This technique relies

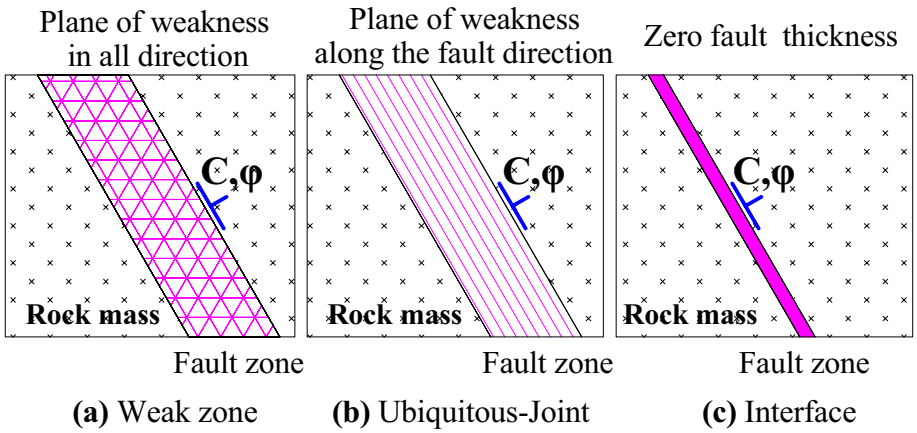

Fig. 1 Fault material modeling methods: **a** weak zone (no preferred plane of weakness, isotropic material), **b** ubiquitous-joint (non-isotropic material), **c** interface (discontinuous face)

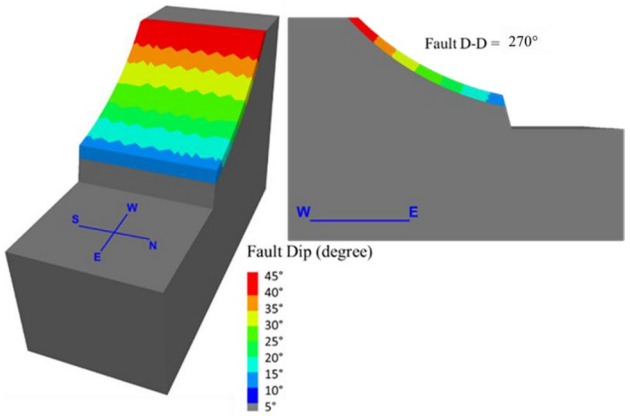

Fig. 2 Contours of dip angle along the fault plane captured by the UJ method (Azarfar 2019)

on a mobilized or failed slope (assuming FOS = 1.0) to calibrate the accuracy of the computational model. In the lack of such a condition (failed slope or accurate displacement measurements), to the best of the authors' knowledge, there appears to be no available laboratory technique for evaluating the capability of fault models in rock structures. In this paper, a novel laboratory method is proposed to calculate slope FOS and simulate the mechanics of failure in a controlled manner. This experiment is used to calibrate and quantify the error magnitude associated with different numerical modeling approaches. Considering the possible sources of error, choosing an appropriate numerical method in modeling a fault is crucial to avoid under or overestimation of the stability. As much as over-estimation (reporting higher FOS value) risks the stability of the system, under estimation (reporting lower FOS value) may reduce the mineable reserve and profit.

This research studies the influence of fault geometry, mesh density, equilibrium ratio, fault thickness, rock mass dilation, and shear strength properties on the slope stability, obtained from the WZ, UJ and IF methods. In addition to the slope stability, the failure mechanism for each method is estimated in small and large scales. In addition,

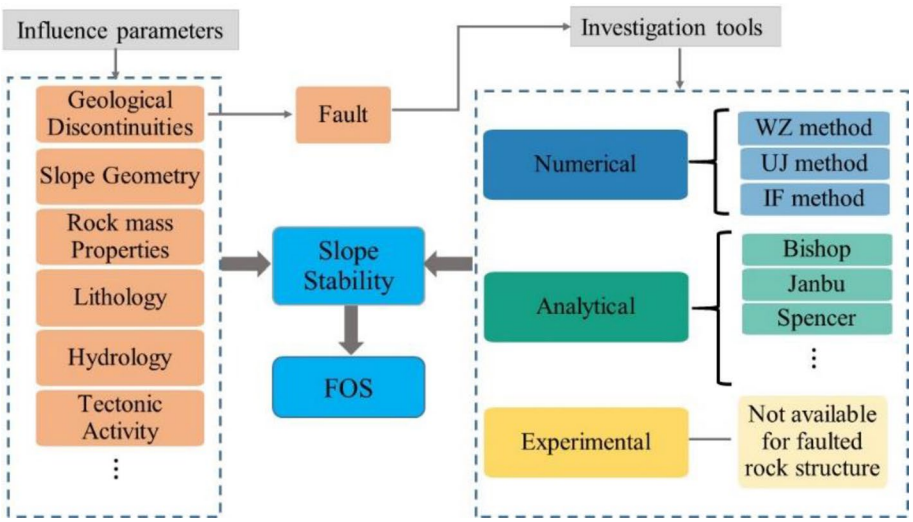

Fig. 3 Schematic modeling of faulted structure and parameters that influence accuracy of the FOS value

a laboratory-scale model is used to evaluate the capability of the numerical method in modeling the stability behavior of the structure.

2 Methodology

In this paper, the WZ, UJ, and IF methods were used to simulate the fault behavior, and the SSR method was used to calculate the FOS values. To reduce the run time, a sensitivity analysis was carried out in the small scale and eventually extended to large-scale modeling. For the small scale, one typical bench of an open-pit mine was simulated, and for the large-scale, the whole open-pit mine was modeled. Laboratory-scale and empirical equations were used to provide a benchmark for modeling results. All simulations were performed in the *FLAC3D* software, in which a finite difference method (FDM) was used.

2.1 Model Configuration

To model the open-pit mine benches, homogeneous isotropic modeling was used. All models were constrained at the bottom (x, y, z direction) and in the normal direction (perpendicular to the side plane) on the sides (N–S and E–W faces). The geometry of the bench was modeled in the Rhino 3D software and then imported to the *FLAC3D* (Fig. 4). The same approach was used for the large-scale model, with the overall pit slope of 44° and bench height of 10 m (Fig. 5).

2.2 Mesh Size Evaluation

For the small- and large-scale modeling, brick elements were used as the dominant mesh geometry, and around the fault plane due to the complexity of the fault shape tetrahedral elements were used (hybrid meshing, Fig. 12). The nodal mixed discretization (NMD) technique that proposed by Marti and Cundall (1982) and described by Abbasi for large-scale simulation was implemented to capture more volumetric flexibility and improve the plasticity of the structure (Abbasi 2016). For all models, the number of tetrahedral per volume of interest (NTV) was set to 60 to create a balance between accuracy and modeling cost (Abbasi et al. 2013).

2.3 Material Properties

The rock mass was modeled as an elastic–plastic material using Mohr–Coulomb failure criterion. Typical properties of a competent rock mass were used in the modeling to ensure the failure happens through the faulted zone (Table 1). The

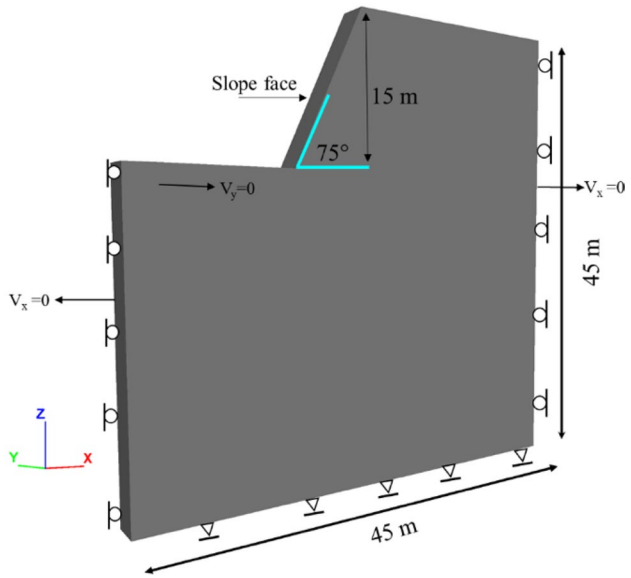

Fig. 4 Small-scale model geometry and boundary conditions

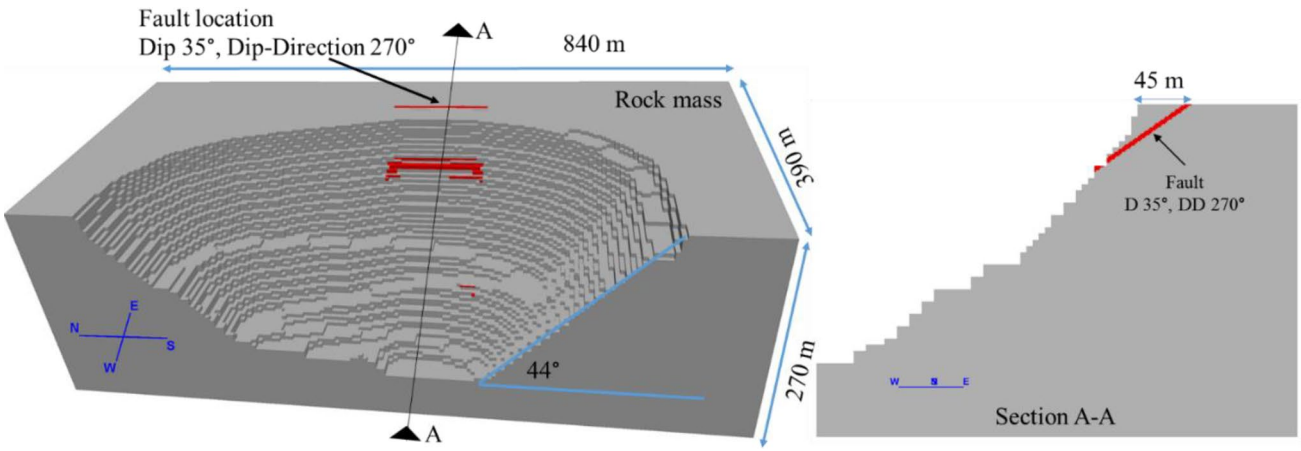

Fig. 5 Large-scale model geometry and boundary conditions

Table 1 Material properties used in numerical modeling

Material properties	Rock mass	Fault	Units
Density	2500	2100	kg m^{-3}
Bulk modulus	3×10^{9}	4.7×10^{7}	Pa
Shear modulus	1.5×10^{9}	3.3×10^{7}	Pa
Cohesion	1×10^{6}	2×10^{4}	Pa
Internal friction angle	36	20	Degree
Tension strength	1×10^{5}	0	Pa
Normal-stiffness	N/A	1×10^{8}	Pa m^{-1}
Shear-stiffness	N/A	0.5×10^{8}	Pa m^{-1}

fault material properties were set similar to those of clayey soil.

2.4 Sensitivity Analysis

The sensitivity analysis was performed by monitoring the stability behavior with respect to changes of different variables in the small-scale faulted structure (single bench) modeled by WZ, IF, and UJ methods. In some sensitivity analyses, parameters such as mesh density and solve ratio are used to find the thresholds above which the stability is independent of parametric changes. Therefore, these thresholds were applied for other sensitivity analyses.

2.4.1 Analysis 1 (Fault Geometry)

A fault trace usually is not straight and usually contains undulations, this may cause interlocking and rock bridges. These features change the fault shear strength and failure mechanics. The effect of fault geometry on the slope stability was analyzed for different geometries: smooth nonplanar, undulated planar, and undulated nonplanar faults (Fig. 6). The goal of this sensitivity study is to evaluate the performance of each numerical method (WZ, UJ and IF) in simulating fault-interlocking behavior.

2.4.2 Analysis 2 (Convergence Ratio – Numerical Stability)

FLAC3D uses an implicit numerical technique for obtaining numerical approximations to the solutions of time-dependent partial differential equations (PDE). Strong convergence criteria are necessary in any numerical scheme for stability of PDE in the initial value problems. Assuming that the PDE is stable, the convergence rate and step size are critical to reach a strong numerical solution (near exact solution). For simplicity in FLAC3D the convergence ratio is called solve ratio and the sensitivity of FOS value with variation of the solve ratio was studied. The solve ratio was allowed to incrementally decrease from 10^{-5} to 10^{-8} to highlight its impact on the FOS value. More details on threshold criteria are discussed in (Azarfar et al. 2018). It should be mentioned that in some cases the number of numerical iterations can also be important in estimating the FOS value.

2.4.3 Analysis 3 (Mesh Density)

In this sensitivity analysis, the FOS of a nonplanar fault was obtained for different mesh densities. It has been shown that higher mesh density in numerical modeling results in higher accuracy, especially in finite element methods (Ghavidel et al. 2018). However, this analysis was performed to

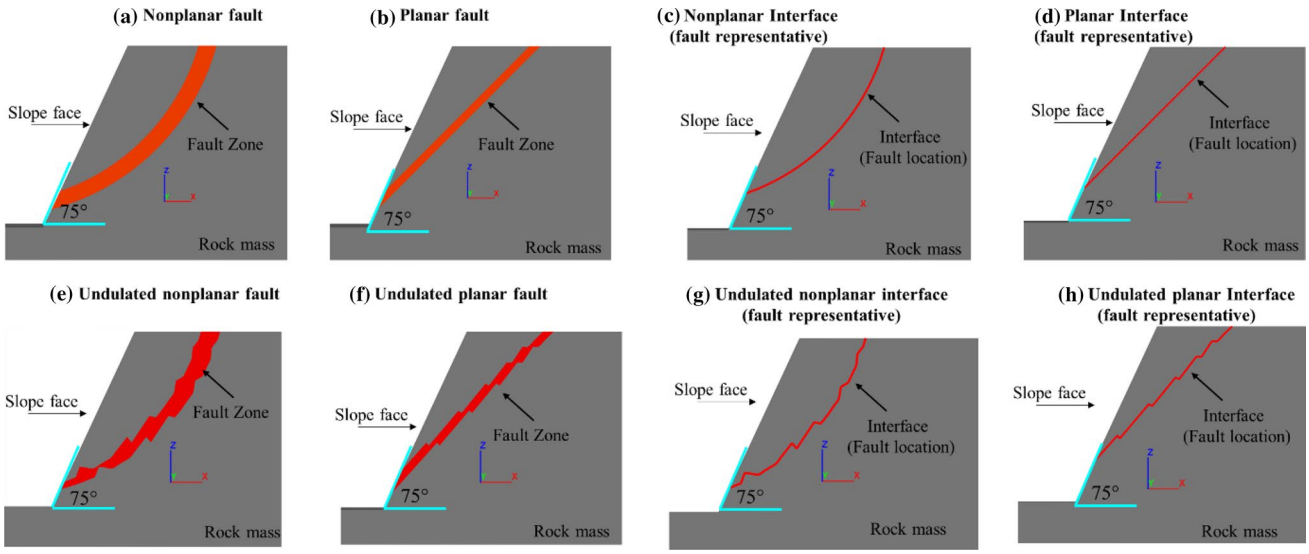

Fig. 6 Different fault geometries: **a** nonplanar fault, **b** planar fault, **c** nonplanar fault (IF), **d** planar fault (IF), **e** undulated nonplanar fault, **f** undulated planar fault, **g** undulated nonplanar fault (IF), **h** undulated planar fault (IF)

approximate a threshold after which the FOS value improvements would not justify the computational burden. Moreover, reaching the small-scale mesh density threshold is not affordable in large-scale modeling and it is essential to approximate the resultant errors.

2.4.4 Analysis 4 (Rock Mass Dilation)

This analysis was carried out to investigate the stability sensitivity to the dilational behavior of the fault zone. This was captured by changing the dilation angle of the fault material using either the corresponding associated or non-associated flow rules. The associated flow rule was used when the dilation angle was equal to the internal friction angle, otherwise, the non-associated flow rule was used.

2.4.5 Analysis 5 (Fault Thickness)

Fault zone thickness is an important parameter for many geotechnical designs. A typical fault thickness can be varied from 1 mm to 10 m and this controls the fault shear displacement. In the fault thickness analysis, the FOS was calculated for different thicknesses of the nonplanar fault. This was performed for the WZ and UJ methods, as the IF, by definition, is in contact with and lacks a separation between the elements of the fault zone. Often, the real thickness of the fault zone cannot be implemented in large-scale modeling due to the mesh density limitation and computational cost.

2.4.6 Analysis 6 (Fault Shear Strength)

Obtaining an intact sample of fault gouge or filling material is very difficult, limited, and requires considerable experience. Using limited and disturbed field samples (or remolded samples) decreases the accuracy of the laboratory tests and design inputs. Sensitivity on the shear strength of the fault material will be a guideline to consider the error associated with the lack of laboratory results. Cohesion and internal friction angle parameters were changed to analyze the sensitivity of each method to the shear strength properties (tension strength = 0) of the fault material. The FOS value was calculated for different inputs of the previously mentioned properties. These parameters will be changed through the SSR process; however, there is always uncertainty in the determination of initial values.

2.5 Theory and Background

2.5.1 Factor of Safety

The SSR method reduces the input cohesion, tensile strength (T_S), and internal friction angle of the material by the same factor (Eq. (2), Fig. 7), and the final strength reduction factor (SRF) represents the FOS (Dawson et al. 1999).

$$\mathrm{FOS} = \mathrm{SRF} = \frac{C_0}{C_\mathrm{r}} = \frac{\tan\varphi_0}{\tan\varphi_\mathrm{r}}. \tag{2}$$

In an iterative manner, the SSR method reduces the strength properties (C_0, T_S and φ_0) by an incremental SRF until a failure happens and repeats this procedure until reaching the smallest intervals within the range of acceptable error. The FOS value for a large open-pit mine is reported usually to no more than two decimals.

2.5.2 Fault Modeling Technique

The following methods were used in the fault modeling of small- and large-scale slopes:

2.5.2.1 Interface (IF) Method In the IF method, the fault material is introduced into the model as planes on which sliding or separation can occur (Fig. 1c). The characteristics of this interface are defined by normal and shear stiffness as well as sliding properties (Itasca 2017). Friction, cohesion, dilation, and tensile and shear bond strength are the properties used in the IF method. The normal and shear stiffness (k_n and k_s) parameters control the elastic deformation normal and along the face of the interface elements. In this study, these parameters were assumed constant. Interface elements introduce a mechanical contact between the two zone surfaces, each of which is defined by three nodes (triangular element). In continuous numerical modeling, the interface elements allow that the two adjacent zones to be separated and behave individually. Equations (3) and (4) show the normal and shear forces at each modeling time step ($t+\Delta t$),

$$F_\mathrm{n}^{(t+\Delta t)} = k_\mathrm{n} u_\mathrm{n} A + \sigma_\mathrm{n} A, \tag{3}$$

$$F_\mathrm{si}^{(t+\Delta t)} = F_\mathrm{si}^{(t)} + k_\mathrm{s} \Delta u_\mathrm{si}^{(t+0.5\Delta t)} A + \sigma_\mathrm{si} A. \tag{4}$$

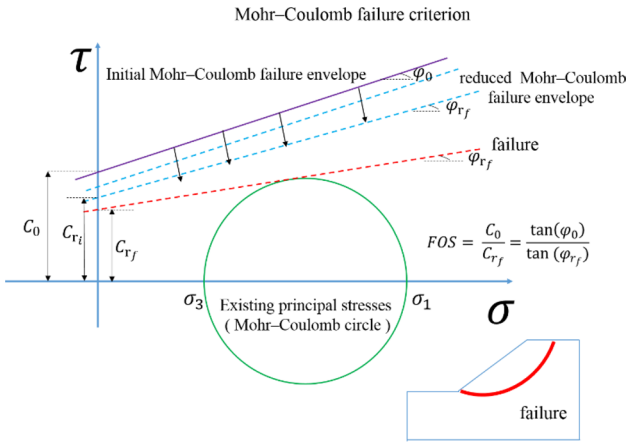

Fig. 7 Shear strength reduction method (Azarfar et al. 2018)

In addition, the maximum shear force is limited by the Coulomb shear-strength criterion and can be calculated by Eq. (5). If the actual shear force is more than the allowable shear force, sliding occurs. The effective normal stress on the discontinuities varies with respect to shear displacement during sliding (Eq. 6).

$$F_{\text{smax}} = cA + \tan\varphi(F_{\text{n}} - pA), \tag{5}$$

$$\sigma_{\text{ni}} = \sigma_{\text{n}} \frac{|F_{\text{s}}|_{\text{o}} - F_{\text{smax}}}{Ak_{\text{s}}} \tan\psi k_{\text{n}}. \tag{6}$$

2.5.2.2 Weak Zone (WZ) Method In the WZ method (Fig. 1a), the fault material and properties are treated as an isotropic medium (with no preference plane of weakness). In other words, the fault mechanical properties were assigned to the zone without defining the dip and dip-direction of the fault plane. In this study, the WZ failure envelope follows the Mohr–Coulomb criterion (shear yield function) with a tension cutoff (tension yield function). On this envelope, the non-associated and associated flow rules, respectively, control the position of a stress point for shear and tension failures (Itasca 2017).

2.5.2.3 Ubiquitous-Joint (UJ) Method The UJ method introduces a specific dip and dip-direction as a virtual weak plane for the fault material (Fig. 1b). It is important to realize this method does not introduce a single plane of weakness, whereas the zone/material has weaker properties in a specific direction (anisotropic behavior). The failure criterion for the plane consists of a composite Mohr–Coulomb envelope with a tension cutoff. The non-associated and associated flow rules control the respective positions of a stress point for shear and tension failures (Jiang 2009; Itasca 2017). The UJ method only represents the simple shear, which differs from the direct shear. In the UJ method, the relevant plastic corrections are made after general failure is detected. Slip will occur on the discontinuity if the following condition is satisfied (Sainsbury and Sainsbury 2017):

$$1 - \tan\varphi_{\text{j}} \ \tan\beta > 0, \tag{7}$$

$$\sigma_1 \geq \sigma_3 + \frac{2(c_{\text{j}} + \sigma_3 \tan\varphi_{\text{j}})}{(1 - \tan\varphi_{\text{j}} \tan\beta)\sin 2\beta}. \tag{8}$$

Based on Eqs. (7) and (8), if $1 - \tan\varphi_{\text{j}} \ \tan\beta < 0$, slip occurs in the rock mass rather than discontinuity. In other words, failure cannot happen along the discontinuities if $\beta < \varphi$ or $\beta = 90$. Also, the normal and shear stress on the joint can be calculated from,

$$\sigma_{\text{n}} = \frac{1}{2}(\sigma_1 + \sigma_3) + \frac{1}{2}(\sigma_1 - \sigma_3)\cos 2\beta, \tag{9}$$

$$\tau = c_{\text{j}} + \sigma_{\text{n}} \tan\varphi_{\text{j}}, \tag{10}$$

$$\tau = \frac{1}{2}(\sigma_1 - \sigma_3)\sin 2\beta, \tag{11}$$

$$\sigma_1 - \sigma_3 = \frac{2(c_{\text{j}} + \sigma_3 \tan\varphi_{\text{j}})}{(1 - \cos\beta \tan\varphi_{\text{j}})\sin 2\beta}. \tag{12}$$

2.6 Laboratory Tests

Two bench samples were built in the laboratory (non-cohesive planar and nonplanar faults) using concrete to evaluate the fault modeling techniques (IF, WZ and UJ) (Fig. 8). For a non-cohesive material, friction angle is the most important factor governing the failure mechanism. The friction angle of the planar model was measured according to the US Bureau of Reclamation (USBR 6258-09) standards, using a manual tilt desk and a digital clinometer. This measurement was repeated (90 measurements, standard deviation-SD = 0.549) to ensure a reasonable precision for the results. The median value of the friction angle and the measured dip angle were used to calculate the FOS based on an analytical formulation (Eq. 13). To make a comparison between simulation and experiment, two samples with the same properties were modeled in FLAC3D software, based on the laboratory-made models (Fig. 8). To adjust the size and geometrical compatibility between the simulation and laboratory models, the latter was 3D-scanned (Artec Spider 3D scanner, accuracy = 0.05 mm, resolution = 0.1 mm) and then transferred to the modeling software. Figure 9 shows the test procedure of 3D scanning for the nonplanar sample. A pull test was performed to obtain the force required for failure in the laboratory (Fig. 10). This force was also calculated from Eq. (14) and compared with the pull force of the planar model to find the correction factor. The correction factor was used to calibrate the failure pull force of the nonplanar model, for which the formula (Eq. 14) is not directly applicable.

$$\text{FOS} = \frac{cA + W\cos\beta\tan\varphi}{W\sin\beta} \underset{c=0}{\Rightarrow} \text{FOS} = \frac{\tan\varphi}{\tan\beta}, \tag{13}$$

$$\text{FOS} = \frac{(W\cos\beta - F\sin\beta)\tan\varphi}{W\sin\beta + F\cos\beta} \tag{14}$$

3 Results and Discussion

3.1 Analysis 1 (Fault Geometry)

The sensitivity results of FOS values for planar, nonplanar, and undulated faults simulations are shown in Fig. 11. The results demonstrate high sensitivity of FOS for the UJ method for nonplanar geometry (about 35% higher that IF

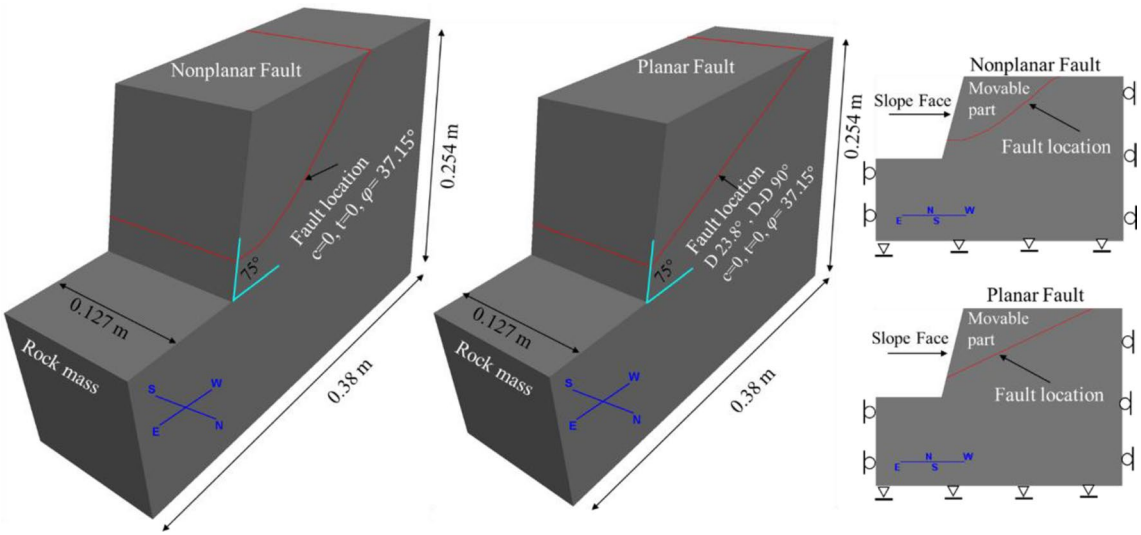

Fig. 8 Laboratory-scale model geometry and boundary conditions

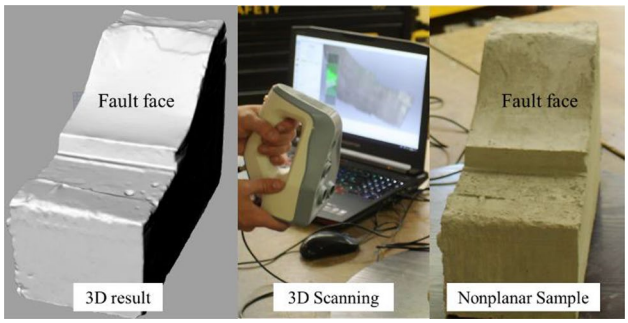

Fig. 9 3D scanning of the lab-scale nonplanar fault model

method). This is due to changes in the angle of discontinuity (β) from 10° to 90° in the undulating faults. Recall that considering Eqs. (7) and (8) for β less than the friction angle and β equal to 90°, failure cannot happen along the plane of weakness (nor through the rock mass since the shear strength is high, Table 1), and, as a result, the UJ method shows artificially higher value of FOS. In addition, the results for undulating nonplanar and planar faults indicate the limitation of the UJ method in capturing the FOS because of the rapid change of β. The same trend was observed in the laboratory testing (discussed in Sect. 3.9).

The WZ method shows increase of the FOS value by introducing undulation due to possible interlockings. The FOS was increased by 3% and 5% for undulating nonplanar and planar fault geometries, respectively. The analysis does not show high sensitivity in the WZ method. In contrast, the IF method shows increase of the FOS values by 13% and 18% for undulating nonplanar and planar fault geometries, respectively; which indicates advantage of using the IF method for undulated fault plane (Fig. 12).

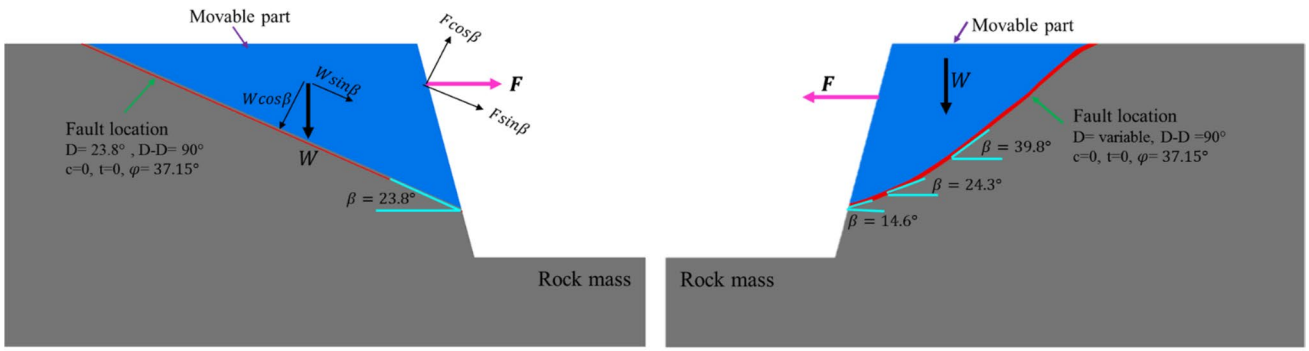

Fig. 10 Laboratory pull test procedure and parameters

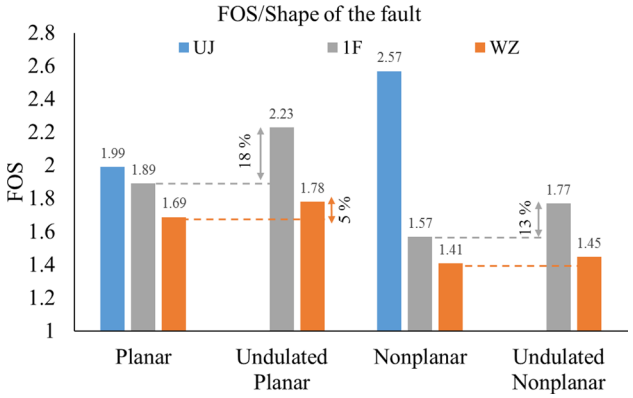

Fig. 11 Fault roughness effect on the FOS for weak zone (WZ), interface (IF), and ubiquitous-joint (UJ) methods

3.2 Analysis 2 (Convergence Ratio – Numerical Stability)

Figure 13 shows the effect of changes in the convergence ratio (10^{-5} to 10^{-8}) on the FOS values for the nonplanar and planar fault. The results indicate that in both planar and nonplanar faults, the FOS values reduce synchronously with decreasing the solve ratio (stronger convergence criteria). However, beyond a certain convergence ratio, below 10^{-7}, this change is negligible (less than 5%) in all three methods. The sensitivity of the IF and WZ methods regarding the convergence ratio is negligible; however, the UJ method shows more sensitivity to the input solve ratios as it cannot capture the correct behavior of continuous features. The results for the nonplanar fault (Fig. 13a) indicate that the optimum threshold for the convergence ratio is different for each method and by knowing this value it is possible to reduce computational cost and time without decreasing the accuracy of the results. In the case of planar faults (Fig. 13b), none of the studied methods exhibit a high sensitivity to the convergence ratio. It is concluded that the optimum threshold for the convergence ratio not only depends on the method of fault material simulation but it also depends on the fault geometry.

3.3 Analysis 3 (Mesh Density)

The computational cost of increasing the mesh density scales as $\sim N^3$, where N is the number of nodal points. In modeling of a large scale open-pit mine with several faults and geological features, increasing the number of nodal points (decreasing mesh size) to eliminate mesh dependency is practically impossible. For example, modeling half of an open-pit mine with dimensions of $1000 \times 500 \times 400$ m and mesh size of 4 m requires 3,125,000 elements, decreasing the mesh size to 2 m, which it is still not ideal, increases the number of elements to 25,000,000. Currently, no supercomputer can handle this calculation in a reasonable time.

The results of mesh density sensitivity analysis (Fig. 14) indicate that the FOS values are insensitive to the mesh density in the WZ method (the accuracy of FOS values improves by less than 5% with a ~ 10 times increase in the mesh density). However, this method is the most conservative technique (lowest FOS value) and low sensitivity to

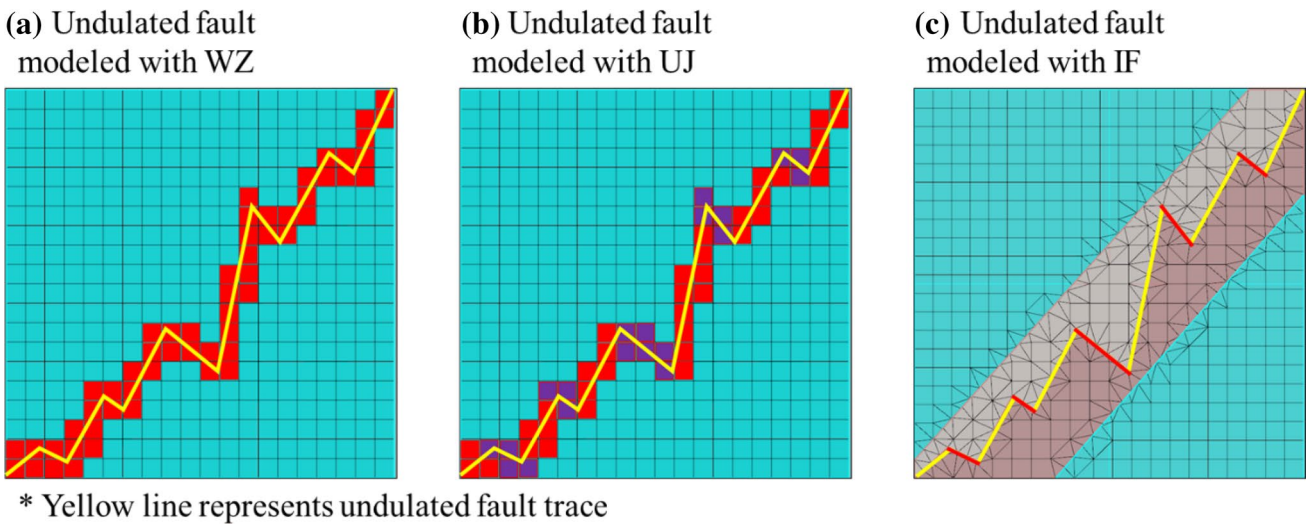

Fig. 12 Undulated fault modeling, **a** WZ method: the red mesh elements show the faulted zone. This method cannot consider the dip angle and direction of undulation; **b** JU method: the red and purple mesh elements show the fault trace. The purple zones represent undulation's dip angle and direction. This method can capture the effect of undulation in FOS value; and **c** IF method: yellow and red lines show the trace of fault. The red section represents fault undulation. This method can also capture the effect of undulation in FOS value (the elements around the fault show the hybrid mesh) (color figure online)

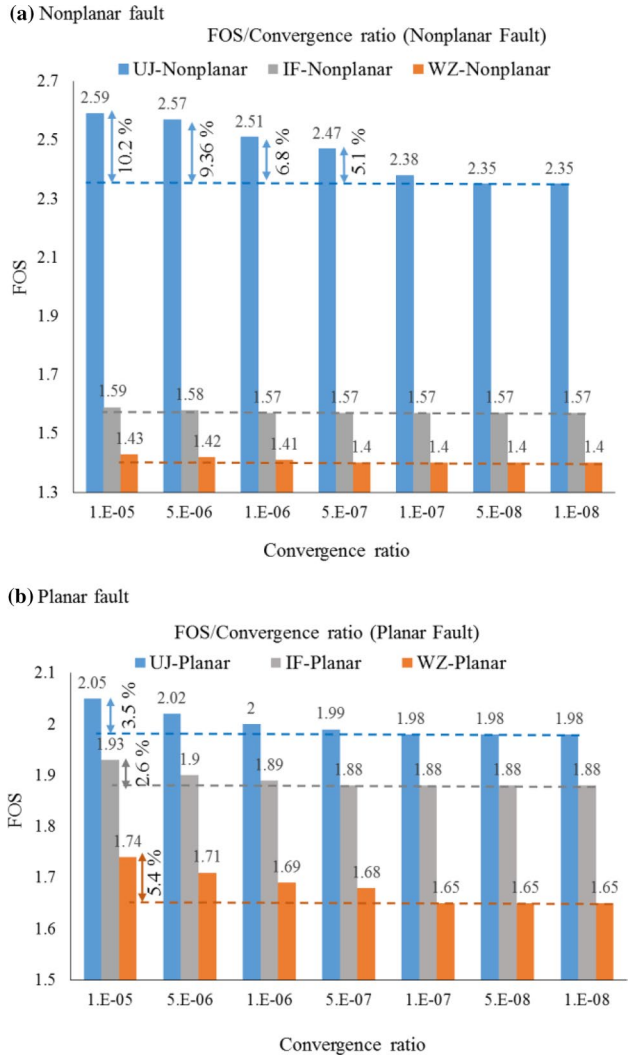

Fig. 13 Dependency of FOS on the convergence ratio, **a** nonplanar fault, **b** planar fault

mesh size does not indicate the quality of the method. The IF method shows median sensitivity in comparison to the two other methods, regarding the mesh size (mesh density). The accuracy of FOS values improves by less than 5% with a ~ 10 times increase in the mesh density (Fig. 14). This is because the IF method relies on contact mechanics and it is mostly independent for the mesh density. The UJ method is the most sensitive, to the mesh density; the accuracy of its FOS values improves by ~ 31% with a ~ 10 times increase in the mesh density. In Fig. 14, the number of zones is an indicator of mesh density, as the dimension of the model is fixed (small scale). The error of FOS with respect to the number of elements was estimated based on the reliable threshold for all three methods (number of elements = 9000). In addition, Fig. 14 shows that the optimum mesh density threshold for each method could be different.

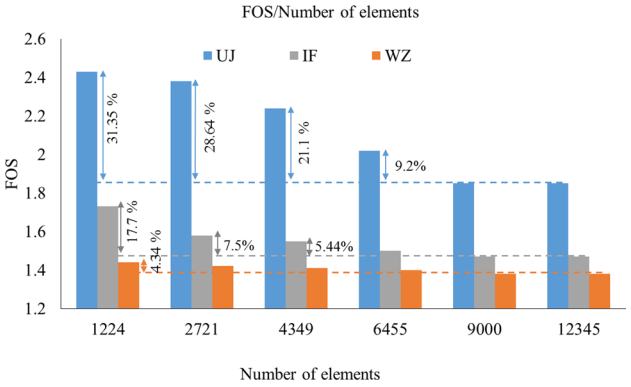

Fig. 14 Mesh density sensitivity analysis for the nonplanar fault

3.4 Analysis 4 (Rock Mass Dilation)

The sensitivity of FOS values to variation of dilation angles (0°–20°) for the nonplanar fault is represented in Fig. 15. The results demonstrate that the FOS values are fairly independent of dilation angle in all methods. This is due to the fact that the Mohr–Coulomb method applies the dilation properties only after failure (local or global). However, it can be argued that in a complex geotechnical model where a structure partially fails, i.e. weak materials fail but do not result in instability, the dilation would change the FOS value. The effect of dilation in such a scenario is beyond the scope of this paper and requires future research.

3.5 Analysis 5 (Fault Thickness)

The thickness of a fault plate is an important parameter for understanding the strength and fault behavior (displacement). The fault thickness can be varied from a few millimeters (clean face) to several meters with gouge and fill materials. Due to mesh size limitation which was explained in the mesh density analysis, it is difficult to capture the correct fault thickness in the modeling. In WZ and UJ method the minimum fault thickness can be one element and in the IF method, the fault thickness cannot be represented.

The FOS results for different fault thicknesses are shown in Fig. 16 for all methods other than IF; thickness does not apply to the IF method. As expected, the results show that increasing the fault thickness reduces the FOS obtained for all the methods, although this reduction is less pronounced for the WZ method. Doubling the fault thickness from 1.5 to 3 meters decreases the FOS by approximately 13% in the UJ method. In this analysis, the initial conditions are set in cautious proximity of imminent failure to compare the bare effect of each method. A more important result is that to capture a current behavior of the fault in the WZ and UJ models, a minimum of three elements is necessary along the thickness of the fault

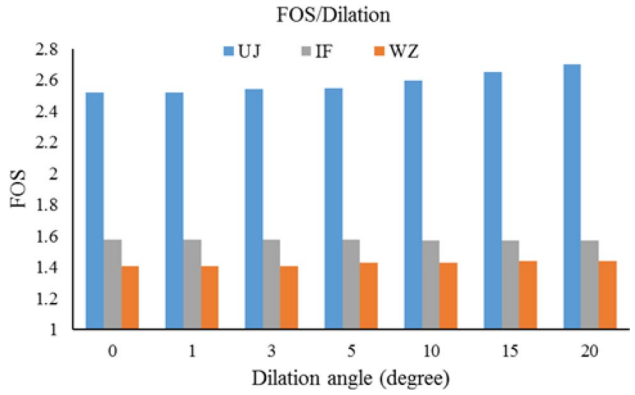

Fig. 15 FOS versus dilation angle for the nonplanar fault

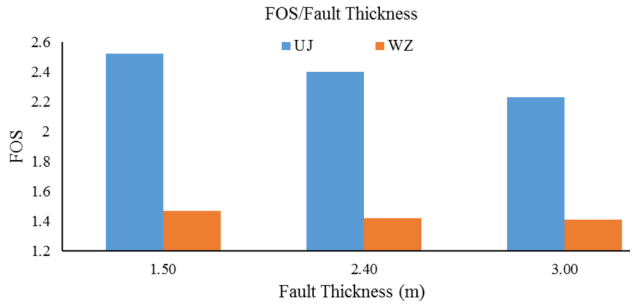

Fig. 16 FOS versus fault thickness for the nonplanar fault

(Fig. 17). One or two elements along the fault show a stiff structure that prevents the movement along the fault plane and unrealistically increases the strength. This is because in the continuum modeling the border fault elements are attached to the adjacent rock mass and the behavior of the elements is a product of the two systems (Fig. 17).

3.6 Analysis 6 (Fault Shear Strength)

A large source of uncertainty can be imposed on the design due to unreliable laboratory tests and lack of representative samples of the potential failure surface. Understanding the sensitivity of FOS value with the shear properties of a fault is important in the better understanding of the modeling result. The sensitivity of the FOS value in response to the changes in cohesion ($c = 0$–45 MPa) and friction angle ($\varphi = 0$–24) is illustrated in Figs. 18 and 19, respectively. As in other analyses, the UJ method indicates the highest sensitivity. As expected, the FOS increases in tune with the increase of shear strength properties. However, this increment is more sensitive to cohesive properties (exponential dependency, dotted lines in Fig. 18) of the fault material rather than its friction angle (linear dependency, dotted lines in Fig. 19). This should be considered in the reduction methods, such as SSR, where cohesion and friction angle are reduced by the same coefficient, whereas a lower coefficient should be given to the more sensitive property, i.e., cohesion. The high cohesion sensitivity can be explained using Eq. 10, for shallow faults the confinement stress is low, and the effect of friction angle ($\sigma_n \tan \varphi_j$) is negligible, however, the reverse is true for a deep fault with high confinement stress.

3.7 Failure Mechanism

In addition to the FOS, the failure mechanism encompasses important information about slope stability. Structural features, such as faults, and discontinuities form the plane of failure. Such surfaces usually are parallel or nearly parallel to the slope face. The sliding plane must daylight in the slope face or the plane would shear into the rock mass. The plane should also intersect the upper surface of the slope or form a tension crack to create a release backplane. Release surfaces that have negligible strength to sliding must be present in the

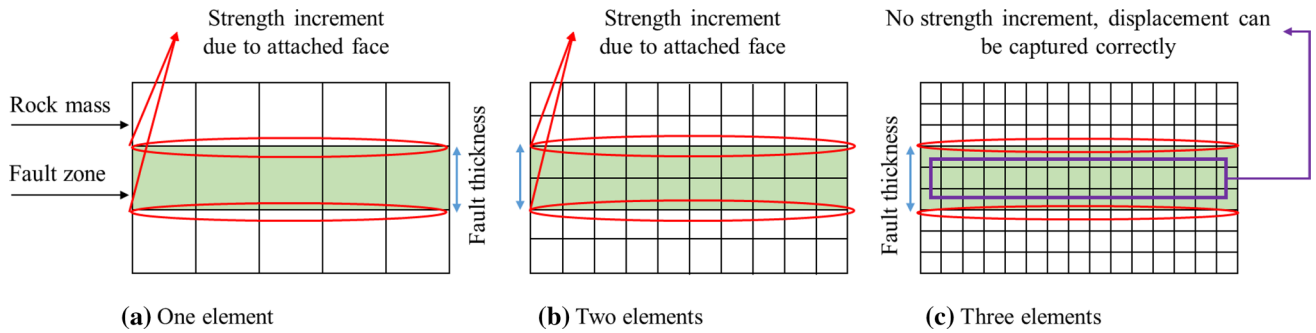

Fig. 17 Effect of the number of elements along the fault thickness (green zone): **a** fault zone modeled with one zone, in this case the upper and lower nodes of the elements are connected to the rock mass and result in the fault having an unrealistic higher strength, **b** fault zone modeled with two zones, in this case the upper and lower nodes of the fault boundary are connected to the rock mass and only the middle nodes are free to move along the fault, and **c** fault zone modeled with three zones, in this case the middle zone and nodes have enough degrees of freedom to move along the fault zone

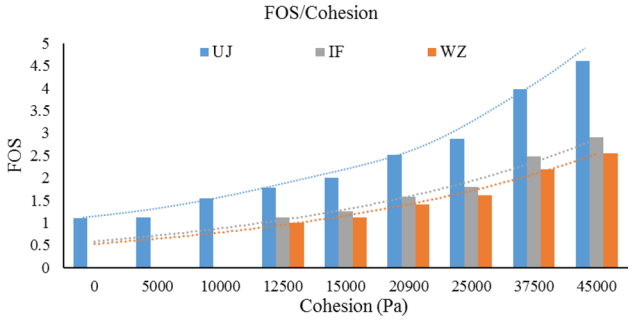

Fig. 18 FOS versus cohesion for the nonplanar fault. The dotted lines show the interpolated trending line for each method. The trend lines show the exponential dependency of FOS to the cohesion change

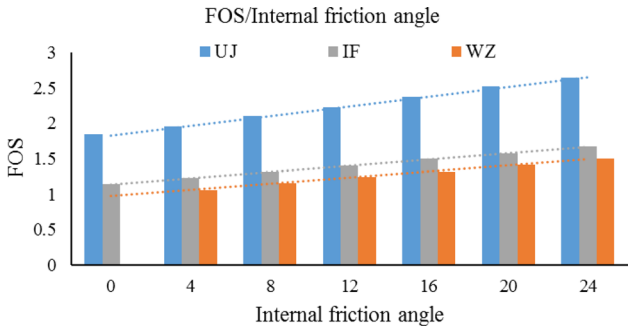

Fig. 19 FOS versus internal friction angle for the nonplanar fault. The dotted lines show the interpolated trending line for each method. The trend lines show the linear dependency of FOS to the internal friction angle change

rock mass to define the lateral boundaries of the slide. Capturing the correct failure mechanism requires a complex and accurate geotechnical and numerical model. The WZ, UJ, and IF introduce faults to the numerical model with different techniques and this may result in capturing different failure surfaces. The failure mechanism predicted by each method is shown in Fig. 20 for all fault geometries. Independent of the fault shape, tension and shear failures occur, respectively, at the bench crest and toe in the WZ (Fig. 20a, b). This shows toppling failure, which is not consistent with the theoretical results. In the UJ (Fig. 20c, d) and IF methods (Fig. 20e, f), however, shear failure is the dominant mechanism throughout the fault. These methods capture the failure mechanism more accurately. Nonetheless, the experience and results imply that the fault modeling methods are intrinsically different, and each suffers from a different set of limitations, making the mechanistic investigations more challenging.

3.8 Large-Scale Results

The proper modeling of the fault by the IF is quite challenging in the large-scale; however, the faults in the whole open-pit mine are modeled using WZ and UJ methods (Figs. 19, 21). The large-scale model is built based on the findings and considerations obtained from the small-scale modeling. Similar to the small-scale case, applying the UJ method results in higher values for the FOS (2.18) compared to the WZ method (1.38). The difference between the FOS value for WZ and UJ is 36% and 15%, respectively, for large scale and small scale. The variation of the FOS value for the bench scale model (small model) is negligible, but it is not within the acceptable range of error for the large scale model. This shows that selecting an appropriate modeling technique is critical for large open-pit mine modeling. Figures 21 and 22 show the displacements in the fault zone modeled, respectively, by WZ and UJ methods. It can be deduced from the FOS values that the UJ model has higher displacements, but both the WZ and UJ models have their maximum displacements at the toe of the fault. This implies that the failure initiates at the bottom of the fault, and both shear and tension participate in the failure mechanism. This failure mechanism is better captured in Fig. 23 (WZ) and Fig. 24 (UJ); in both figures, shear is dominant in the fault zone (i.e. slipping along fault plane). Massive tension failure is shown in the WZ model within the mobilized rock mass. Similar to the small scale model, this can be an indicator of toppling failure, which is not realistic.

3.9 Laboratory Results

The median value of the friction angle of the laboratory models with a planar fault (STDEV = 0.549 for 90 measurements) is 37.15°. With this friction angle and dip angle of 23.8°, and using Eq. (13), the FOS is 1.718. Identical geometry and material properties were used to simulate the laboratory test model in FLAC3D software. A comparison between this FOS value and those of the scanned model ($FOS_{lab} = 1.71$, $FOS_{WZ} = 1.51$, $FOS_{IF} = 1.62$, and $FOS_{UJ} = 1.76$) indicates a good agreement between the UJ and IF methods and the laboratory model (~ 3–5% discrepancy, Table 2). This agreement is not surprising, as all the properties of the laboratory model are exactly transferred to the software, including zero cohesion for the fault zone. Calibration between the median force obtained from the pull test of the planar laboratory model and the force required for imminent failure from Eq. (14) results in a 0.925 correction factor (STDEV = 0.864 for 134 measurements). In addition, a comparison between the median force obtained from the pull test of the nonplanar laboratory model (normalized by correction factor) and the loading forces of scanned models indicates that the IF and UJ methods are more successful in modeling the failure for non-cohesive faults. These values are 11.90, 10.75, 11.5, and 12.12 N for the normalized median pull force, and the loading forces from the WZ, IF, and UJ models. The summary of the results is shown in

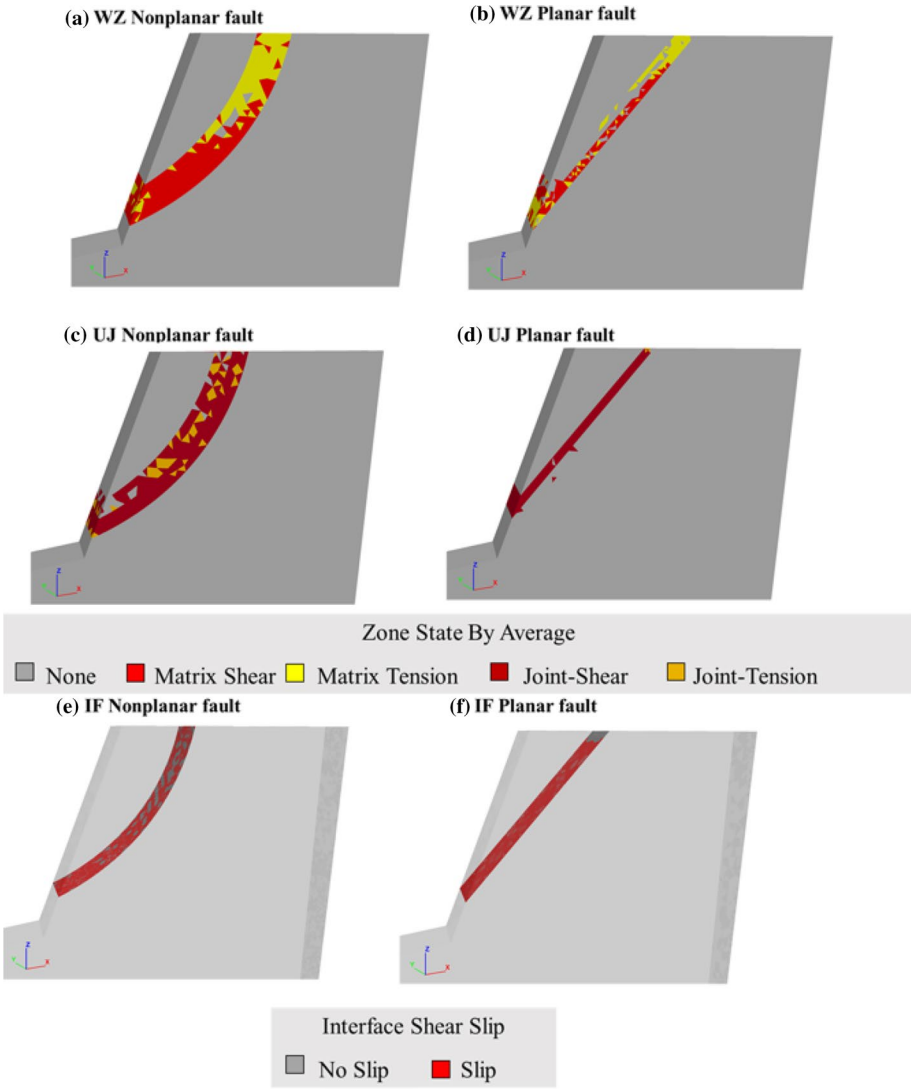

Fig. 20 Failure mechanism of **a** WZ nonplanar, **b** WZ planar, **c** UJ nonplanar, **d** UJ planar, **e** IF nonplanar, and **f** IF planar faults

Table 3. More laboratory tests are needed for the cohesive material and large-scale model.

4 Conclusions

In this study, the slope stability of a single bench in the small and laboratory scales and of a whole open-pit mine in the large-scale are investigated in the presence of fault zones. Comparative and sensitive analyses are performed using three fault modeling methods and different initial conditions, and the effects are studied on the FOS of different models. Among the fault modeling methods, the ubiquitous-joint (UJ) exhibited the highest sensitivity to the initial condition, and the weak zone (WZ) exhibited the lowest. This trend was almost the same for the magnitude of the resulting FOS obtained by the latter two methods. Although the UJ method requires more information in the fault modeling, its high sensitivity suggests this method's better capability only when initial conditions are reliably collected. Moreover, the UJ method is incapable of representing direct shear and, thus, the correct behavior of continuous features. Especially in undulating nonplanar models, the UJ method cannot capture the failure in the fault zone and consequently overestimates the FOS. The mesh density analysis indicates that after a certain threshold, the higher resulting accuracy is negligible compared to the increase of the computational cost. A comprehensive comparison of the three numerical methods for the fault material simulation is summarized in Table 4. This study

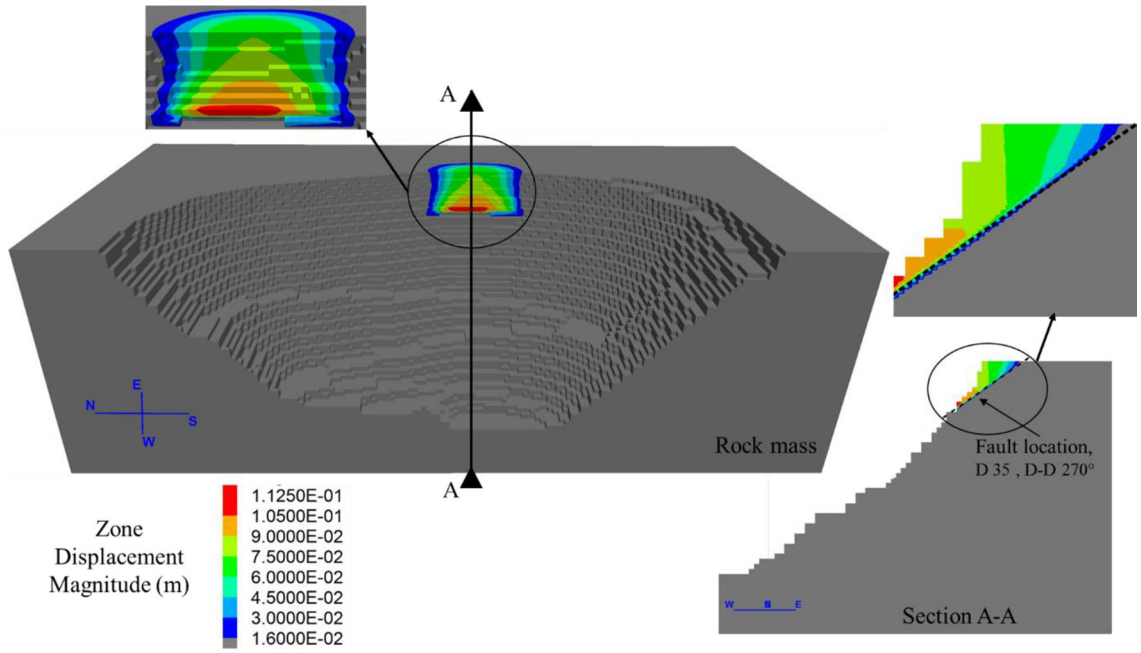

Fig. 21 Displacement contours, using WZ method. The black dashed line demarcates the fault location

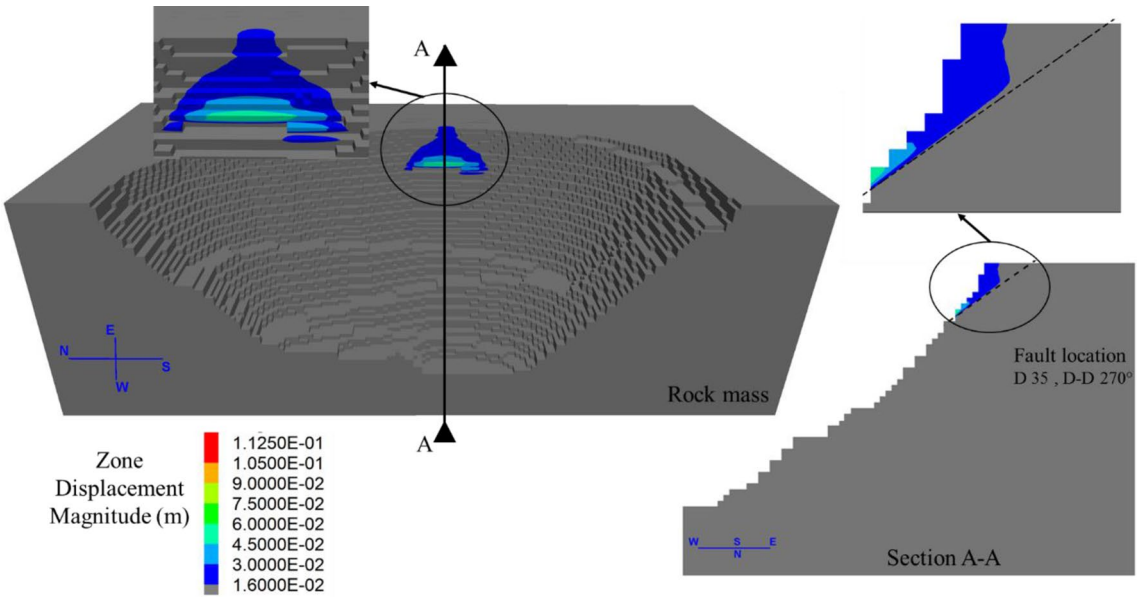

Fig. 22 Displacement contours, using UJ method. The black dashed line demarcates the fault location

infers that cohesion and friction angle should not have the same reduction factor in the SSR method, as their efficacy on the FOS suggests. The large-scale modeling implies the initiation of failure from the bottom of the fault, propagation of shear stress along the fault, and tension stress towards the rock mass. A comparison between numerical and laboratory experiments indicates a better agreement between the two when the UJ and IF methods are used. However, more laboratory tests are under investigation to increase the level of sophistication and comparability between the theoretical and experimental stability tests on rock material.

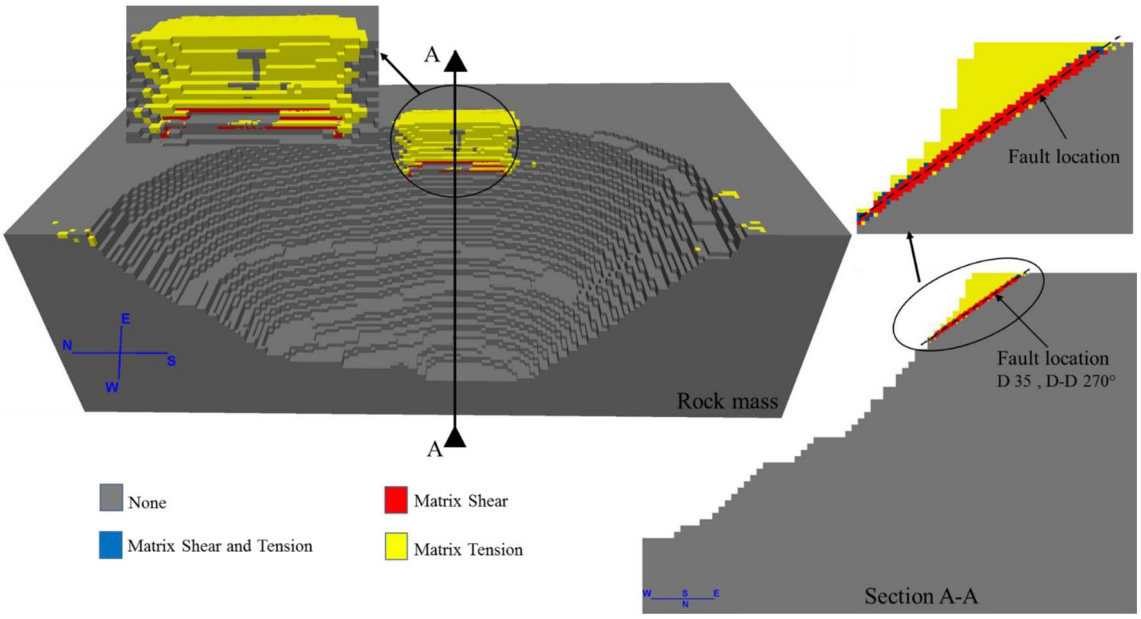

Fig. 23 Failure mechanism obtained by WZ method. The black dashed line demarcates the fault location

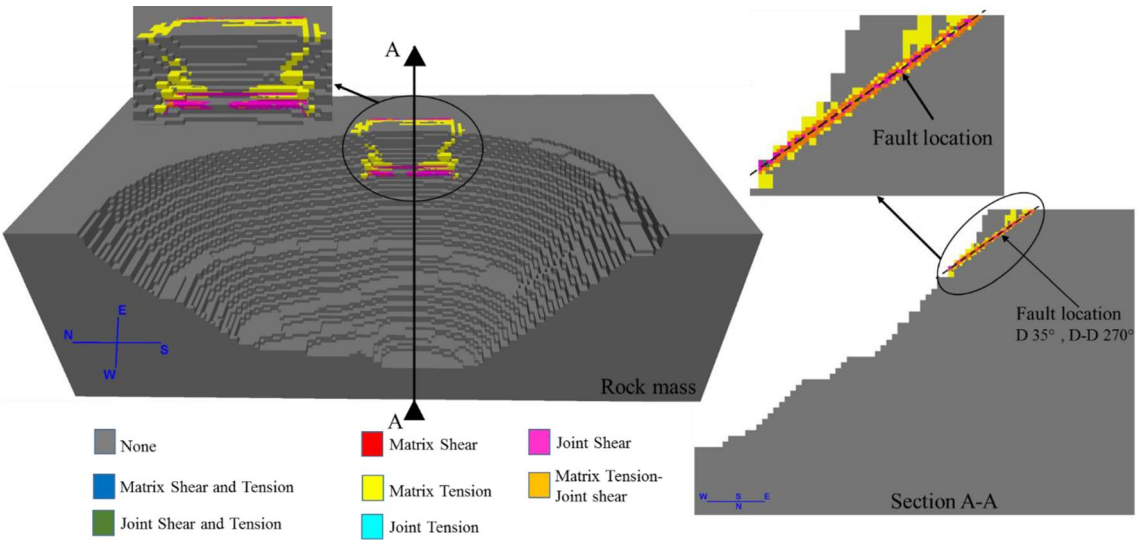

Fig. 24 Failure mechanism obtained by UJ method. The black dashed line demarcates the fault location

Table 2 Summary of the calculated FOS for planar sample

	Numerical modeling			Laboratory
	WZ	IF	UJ	Analytical
FOS	1.51	1.62	1.76	1.71
Error (%)	−11.7	−5.27	2.93	N/A

Table 3 Summary of the pull test results for the nonplanar sample

	Numerical modeling			Laboratory
	WZ	IF	UJ	Direct measurement
Force required for imminent failure (N)	10.75	11.5	12.12	11.9
Error (%)	−9.67	−3.37	1.85	N/A

Table 4 Comprehensive comparison of three numerical methods for fault material simulation

Method	Advantage	Disadvantage	Comments
Weak zone	Easy to build complex geometry Conservative method for estimating FOS value Suitable method when working with low accurate data Low sensitivity to mesh size Low sensitivity to solve ratio	Possibility of the underestimate of FOS, especially in large scale and complex modeling Cannot capture the orientation of discontinuities Cannot capture correct mechanism of failure (tend to show toppling behavior) Requires at least three elements along fault thickness to capture displacement Shows lowest consistency with the laboratory results	The lowest sensitivity with respect to the input parameters, and fault geometry This technique does not require high experience to build the model
Ubiquitous-joint	Considers the orientation of the planes of weakness (dip and dip-direction) Relatively easy to build complex geometry Captures correct mechanics of failure Good correlation with laboratory results	Possibility of the overestimate of FOS value Sensitive to solve ratio, it requires low convergence value Cannot consider the joint spacing, length and stiffness Cannot capture the correct behavior of continues feature High sensitive to mesh size Requires at least three elements along fault thickness to capture displacement	Highest sensitivity with respect to the input parameters, and fault geometry
Interface	Can model the actual mechanical separation Considers the orientation of the planes of weakness (dip and dip-direction) Captures correct mechanics of failure Good correlation with laboratory results Low sensitivity to mesh size Low sensitivity to solve ratio	Cannot consider the fault zone thickness Very difficult to build complex geological structures	Medium sensitivity with respect to the input parameters, and fault geometry This method requires high level of expertise to build the complex geometry

Acknowledgements This work was funded by the University of Nevada, Reno (PG11522). Authors thank Dr. Jaak Daemen Dr. Pierre Mousset-Jones and Dr. Loren Lorig (Itasca International Company) for peer-reviewing the paper. Also, authors would like to thank journal's editor and reviewers.

References

Abbasi B (2016) An improved rock mass behavior numerical model and its applications to longwall coal mining. Southern Illinois University, Carbondale

Abbasi B, Russell D, Taghavi R (2013) FLAC3D mesh and zone quality. In: FLAC/DEM symposium. Itasca Consulting Group, China

Alejano LR, Alonso E (2005) Considerations of the dilatancy angle in rocks and rock masses. Int J Rock Mech Min Sci 42:481–507. https://doi.org/10.1016/j.ijrmms.2005.01.003

Alzo'ubi AK (2016) Modeling yield propagation of jointed synthetic rock. In: Rock mechanics and rock engineering: from the past to the future. CRC Press, Taylor and Francis Group, Boca Raton

Azarfar B (2019) Numerical and experimental analysis of the effect of faults in open-pit mining stability. University of Nevada, Reno

Azarfar B, Peik B, Abbasi B, Roghanchi P (2018) A discussion on numerical modeling of fault for large open pit mines. American Rock Mechanics Association, Seattle (Document ID: ARMA-2018-080)

Bishop AW (1955) The use of the slip circle in the stability analysis of slopes. Géotechnique 5:7–17. https://doi.org/10.1680/geot.1955.5.1.7

Cala M, Flisiak J, Tajdus A (2006) Slope stability analysis with FLAC in 2D and 3D. In: 4th International FLAC symposium on numerical modeling in the geomechanics, Madrid

Dawson EM, Roth WH, Drescher A (1999) Slope stability analysis by strength reduction. Géotechnique 49:835–840. https://doi.org/10.1680/geot.1999.49.6.835

Duncan JM (1996) State of the art: limit equilibrium and finite-element analysis of slopes. J Geotech Eng 122:577–596. https://doi.org/10.1061/(ASCE)0733-9410(1996)122:7(577)

Fleurisson J-A (2012) Slope design and implementation in open pit mines: geological and geomechanical approach. Procedia Eng 46:27–38. https://doi.org/10.1016/j.proeng.2012.09.442

Franz J (2009) An investigation of combined failure mechanisms in large scale open pit slopes. University of New South Wales, Sydney

Ghavidel A, Mousavi SR, Rashki M (2018) The effect of fem mesh density on the failure probability analysis of structures. KSCE J Civ Eng 22:2370–2383. https://doi.org/10.1007/s12205-017-1437-5

Gupta V, Bhasin RK, Kaynia AM et al (2016) Finite element analysis of failed slope by shear strength reduction technique: a case study for Surabhi Resort Landslide, Mussoorie township, Garhwal Himalaya. Geomatics Nat Hazards Risk 7:1677–1690. https://doi.org/10.1080/19475705.2015.1102778

Hammah R., Yacoub T, Corkum B et al (2007) Analysis of blocky rock slopes with finite element shear strength reduction analysis. In: 1st Canada-U.S. rock mechanics symposium, Vancouver, pp 329–334

Itasca (2017) FLAC3D (fast lagrangian analysis of continua in 3 dimensions)

Jiang Q (2009) Strength reduction method for slope based on a ubiquitous-joint criterion and its application. Min Sci Technol 19:452–456. https://doi.org/10.1016/S1674-5264(09)60084-3

Marti J, Cundall P (1982) Mixed discretization procedure for accurate modelling of plastic collapse. Int J Numer Anal Methods Geomech 6:129–139. https://doi.org/10.1002/nag.1610060109

Matsui T, San K (1992) Finite element slope stability analysis by shear strength reduction technique. Soils Found 32:59–70. https://doi.org/10.3208/sandf1972.32.59

Mostyn G, Helgstedt MD, Douglas KJ (1997) Towards field bounds on rock mass failure criteria. Int J Rock Mech Min Sci 34:208.e1–208.e18. https://doi.org/10.1016/S1365-1609(97)00163-9

Park D, Michalowski RL (2017) Three-dimensional stability analysis of slopes in hard soil/soft rock with tensile strength cut-off. Eng Geol 229:73–84. https://doi.org/10.1016/j.enggeo.2017.09.018

Raghuvanshi TK (2019) Plane failure in rock slopes—a review on stability analysis techniques. J King Saud Univ Sci 31:101–109. https://doi.org/10.1016/j.jksus.2017.06.004

Sainsbury BL, Sainsbury DP (2017) Practical use of the ubiquitous-joint constitutive model for the simulation of anisotropic rock masses. Rock Mech Rock Eng 50:1507–1528. https://doi.org/10.1007/s00603-017-1177-3

Sjoberg J, Hustrulid WA, McCarter MK, Van Zyl DJA (2000) Failure mechanisms for high slopes in hard rock. In: 4th International conference on stability in open pit mining. Society for Mining, Metallurgy, and Exploration, Littleton, pp 71–80

Stacey T, Xianbin Y, Armstrong R, Keyter G (2003) New slope stability considerations for deep open pit mines. J South Afr Inst Min Metall 103:373–390

Stead D, Wolter A (2015) A critical review of rock slope failure mechanisms: the importance of structural geology. J Struct Geol 74:1–23. https://doi.org/10.1016/j.jsg.2015.02.002

Sun C, Chai J, Xu Z et al (2016) Stability charts for rock mass slopes based on the Hoek–Brown strength reduction technique. Eng Geol 214:94–106. https://doi.org/10.1016/j.enggeo.2016.09.017

Taleb Hosni A, Berga A (2016) Assessment of slope stability by continuum and discontinuum methods. In: 18th International conference on civil and geological engineering, Istanbul

Tang SB, Huang RQ, Tang CA et al (2017) The failure processes analysis of rock slope using numerical modelling techniques. Eng Fail Anal 79:999–1016. https://doi.org/10.1016/j.engfailanal.2017.06.029

Tutluoglu L, Ferid Öge I, Karpuz C (2011) Two and three dimensional analysis of a slope failure in a lignite mine. Comput Geosci 37:232–240. https://doi.org/10.1016/j.cageo.2010.09.004

Vermeer PA (1998) Non-associated plasticity for soils, concrete and rock. Physics of dry granular media. Springer Netherlands, Dordrecht, pp 163–196

Wiles T (2014) Three ways to assess mining-induced fault instability using numerical modelling, The Southern African Institute of Mining and Metallurgy 6th South African Rock Engineering Symposium SARES 2014

Yang P, Zhu ZY, Zou ZY (2012) Study on strength reduction method with two reduction-factors. Appl Mech Mater 204–208:429–433. https://doi.org/10.4028/www.scientific.net/AMM.204-208.429

You G, Al Mandalawi M, Soliman A et al (2017) Finite element analysis of rock slope stability using shear strength reduction method. International Congress and Exhibition "Sustainable Civil Infrastructures: Innovative Infrastructure Geotechnology". Springer, Cham, pp 227–235

Zhang K, Cao P, Liu Z et al (2011) Simulation analysis on three-dimensional slope failure under different conditions. Trans Nonferrous Met Soc China 21:2490–2502. https://doi.org/10.1016/S1003-6326(11)61041-8

Zheng Y, Chen CX, Zhu XX et al (2013) Stability Analysis of open-pit slope containing a fault utilizing UDEC. Appl Mech Mater 444–445:1204–1210. https://doi.org/10.4028/www.scientific.net/AMM.444-445.1204

Zienkiewicz OC, Humpheson C, Lewis RW (1975) Associated and non-associated visco-plasticity and plasticity in soil mechanics. Géotechnique 25:671–689. https://doi.org/10.1680/geot.1975.25.4.671